Analysis of an Open-Ended Coaxial Probe with Lift-Off for Nondestructive Testing

James Baker-Jarvis, *Senior Member, IEEE*, Michael D. Janezic, *Member, IEEE*, Paul D. Domich, and Richard G. Geyer, *Senior Member, IEEE*

***Abstract*—The open-ended coaxial probe with lift-off is studied using a full-wave analysis, and an uncertainty analysis is presented. The field equations for the following terminations are worked out: (1) the sample extends to ∞ in the positive axial direction, (2) the sample is backed by a well-characterized material, and (3) the sample is backed by a short-circuit termination. The equations are valid for both dielectric and magnetic materials. The model allows the study of the open-ended coaxial probe as a nondestructive testing tool. The analysis allows a study of the effects of air gaps on probe measurements. The reflection coefficient and phase are studied as a function of lift-off, coaxial line size, permittivity, permeability, and frequency. Numerical results indicate the probe is very sensitive to lift-off. For medium to high permittivity values and electrically small probes, gaps on the order of fractions of a millimeter strongly influence the reflection coefficient. In order for the field to penetrate through the air gap, larger size coaxial line or higher frequencies need to be used. A comparison of the theory to experiment is presented. The results are in close agreement. A differential uncertainty analysis is also included.**

I. Introduction

OPEN-ENDED COAXIAL PROBES are commonly used as nondestructive testing tools. In most applications the coaxial probe is pressed against a sample, and the reflection coefficient is measured and used to determine the permittivity of the sample. Over the years, the open-ended coaxial probe has been studied extensively both theoretically and experimentally. There is a copious literature, and no attempt at a comprehensive review is attempted here (see for example [1]–[13]). (In the proof stage of this paper we also became aware of additional work performed at the National Physical Laboratory [14], [15].) The method, although nondestructive, does have limitations. For example, the fields at the probe end contain both E_z and E_ρ components. If there is an air gap between sample and probe, the discontinuity in the normal electric field causes a large error in the predicted permittivity. For this reason the probe has been used primarily for liquid and semiliquid measurements, where good contact can be obtained.

Very recently, a number of publications have addressed the layered problem using the full-wave model [9]–[15]. It is important to have a model that will allow the study of the effects of air gap on dielectric measurements. Also, in process control, such as rolling stock on assembly lines, a noncontacting probe may be required. For this reason it is important to have a model of a coaxial probe which includes *lift-off*. This paper reports on a study of the effects of probe size, frequency, and lift-off for obtaining optimal material measurements. To this end we present the full-wave theory for open-ended coaxial probes with an air gap between the ground plane and the material under test. Equations are worked out for various terminations. These terminations include a semi-infinite material, the sample backed by a perfect short circuit, and a material termination.

An open-ended coaxial probe consists of a coaxial line where the outer conductor is flared out into a ground plane as indicated in Fig. 1. The coaxial line with inner dimension a and outer dimension b is filled with a material of permittivity ϵ^*_{Rc} and permeability μ^*_{Rc}. The material under test is assumed to extend to infinity in the radial direction and have a homogeneous and isotropic complex permittivity and permeability

$$\epsilon^*_s = [\epsilon'_{\mathrm{Rs}} - j\epsilon''_{\mathrm{Rs}}]\epsilon_{\mathrm{o}} = \epsilon^*_{\mathrm{Rs}}\epsilon_{\mathrm{o}}, \tag{1}$$

$$\mu^*_s = [\mu'_{\mathrm{Rs}} - j\mu''_{\mathrm{Rs}}]\mu_{\mathrm{o}} = \mu^*_{\mathrm{Rs}}\mu_{\mathrm{o}}. \tag{2}$$

Here ϵ_{o} and μ_{o} are the permittivity and permeability of vacuum, and ϵ^*_{Rs} and μ^*_{Rs} are the complex permittivity and permeability of the sample relative to vacuum. The short-circuit termination model allows the realistic modeling of substrate materials which are metal-clad on the bottom. The semi-infinite model is useful for materials thick enough that boundary effects are not important. Finally, the dielectric-terminated geometry is useful when the fields penetrate the sample. The terminations allow measurements to be taken either in strong magnetic fields using a short circuit or in strong electric fields using an open circuit. The field extension from the end of the coaxial line can be controlled by the frequency of operation and coaxial line diameter. At lower frequencies the fields penetrate very little beyond the end of the coaxial probe tip. In such cases it is very hard to obtain good material measurements, particularly magnetic measurements. The goal of this paper is to study the effects of lift-off as a function of probe size, frequency, and material parameters. Also results of permittivity and permeability measurements from an inverse numerical calculation will be presented.

Manuscript received June 4, 1993; revised April 7, 1994.

J. Baker-Jarvis, M. D. Janezic, and R. G. Geyer are with Electromagnetic Fields Division, National Institute of Standards and Technology, Boulder, CO 80303-3328 USA.

P. D. Domich is with the Applied and Computational Mathematics Division, National Institute of Standards and Technology, Boulder, CO 80303-3328 USA.

IEEE Log Number 9404401.

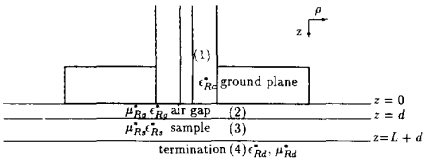

Fig. 1. The open-ended coaxial probe over a sample with an air gap between sample and probe. The cases considered are (1) semi-infinite media, (2) short-circuit termination location at $z = d + L$, and (3) material termination where a well-characterized material occupies the region starting at $z = d + L$ and extending to ∞.

We will assume that the system operates at such a frequency that only the fundamental TEM mode propagates in the coaxial line. Evanescent TM_{0n} modes are also assumed to exist in the coaxial line near the probe end. The existence of TM_{0n} modes in the coaxial line is necessary to match boundary conditions at the probe-material interface. The fields generated in the material under test are primarily reactive; however, radiative fields may also exist. We assume that the probe operates at a known lift-off position. For cases where lift-off is unknown it is possible to operate the probe to obtain relative measurements. In the coaxial line and the material under test the magnetic field is assumed to be azimuthally symmetric. Therefore only the H_ϕ component needs to be calculated.

In the next section we will develop the theory of the probe with lift-off. The method is based on a Hankel transform with respect to the radial coordinate, so the problem is reduced to one dimension. The theory is exact; but, in numerical calculations only a finite number of TM_{0n} modes are used. In the last section, numerical solutions to the equations will be displayed. Numerical solutions, for the case of zero lift-off, will be compared to published results. Finally, the effects of lift-off on the reflection coefficient will be studied.

II. Reflection Coefficient of the Open-Ended Coaxial Probe With Lift-Off

We consider the coaxial probe with an air gap as shown in Fig. 1. The thickness of the air gap is d, and the thickness of the sample is L.

The magnetic field in region (i) as indicated in Fig. 1 satisfies

$$\left[\frac{\partial^2}{\partial\rho^2} + \frac{1}{\rho}\frac{\partial}{\partial\rho} - \frac{1}{\rho^2} + \frac{\partial^2}{\partial z^2} + k_i^2\right] H_{\phi(i)}(\rho, z) = 0. \quad (3)$$

We have assumed a time dependence of $\exp(j\omega t)$. The wave numbers in the coaxial line, gap, material under test, and termination material are $k_1^2 = \epsilon^*_{\mathrm{Rc}}\mu^*_{\mathrm{Rc}}(\omega/c_{\mathrm{vac}})^2$, $k_2^2 = \epsilon^*_{\mathrm{Rg}}\mu^*_{\mathrm{Rg}}(\omega/c_{\mathrm{vac}})^2$, $k_3^2 = \epsilon^*_{\mathrm{Rs}}\mu^*_{\mathrm{Rs}}(\omega/c_{\mathrm{vac}})^2$, $k_4^2 = \epsilon^*_{Rd}\mu^*_{Rd}(\omega/c_{\mathrm{vac}})^2$ respectively, where c_{vac} is the speed of light in vacuum. The boundary conditions are

$$H_{\phi(i)}(\rho \to \infty, z) \to 0, \ (i = 2, 3, 4). \quad (4)$$

$$H_{\phi(2)}(\rho, 0_+) = H_{\phi(1)}(\rho, 0_-) \quad (5)$$

$$H_{\phi(3)}(\rho, d_+) = H_{\phi(2)}(\rho, d_-) \quad (6)$$

$$H_{\phi(4)}(\rho, d + L_+) = H_{\phi(3)}(\rho, d + L_-). \quad (7)$$

In addition, the electric fields are matched at the probe-material interface. For a material termination,

$$H_{\phi(4)}(\rho, z \to \infty) \to 0 \quad (8)$$

and for a short-circuit termination,

$$E_{\rho(3)}(\rho, d + L) = 0. \quad (9)$$

The radial component of the electric field can be calculated from $H_{\phi(i)}$:

$$E_{\rho(i)} = -\frac{1}{j\omega\epsilon_i^*}\frac{\partial H_{\phi(i)}}{\partial z}. \quad (10)$$

It can be shown rather easily that the solution to (3) with boundary conditions (4) through (9) is unique.

A. Fields in Sample and Gap

We will proceed by taking the Hankel integral transform of (3) with respect to ρ. The transformed field is denoted by $\tilde{H}_{\phi(i)}$, where ζ is an eigenvalue corresponding to the radial coordinate. In the air gap, the sample, and the termination material the transformed form of (3) is

$$\left[\frac{d^2}{dz^2} + \left(k_i^2 - \zeta^2\right)\right]\tilde{H}_{\phi(i)} = 0 \quad (11)$$

where i denotes region. We define propagation constants $\gamma_i = j\sqrt{k_i^2 - \zeta^2}$, for $\Re(k_i) > \zeta$, $i = 2, 3, 4$, and $\gamma_i = \sqrt{\zeta^2 - k_i^2}$ if $\Re(k_i) < \zeta$. The Hankel transform we use is defined as

$$\tilde{f}(\zeta) = \int_0^\infty \rho' J_1(\zeta\rho') f(\rho') d\rho' \quad (12)$$

and the inverse transform is defined as

$$f(\rho) = \int_0^\infty \zeta J_1(\zeta\rho)\tilde{f}(\zeta) d\zeta \quad (13)$$

where J_1 is the Bessel function of first kind. The transformed boundary conditions are

$$\tilde{H}_{\phi(2)}(\zeta, 0_+) = \tilde{H}_{\phi(1)}(\zeta, 0_-) \quad (14)$$

$$\tilde{H}_{\phi(3)}(\zeta, d_+) = \tilde{H}_{\phi(2)}(\zeta, d_-) \quad (15)$$

$$\tilde{H}_{\phi(4)}(\zeta, d + L_+) = \tilde{H}_{\phi(3)}(\zeta, d + L_-). \quad (16)$$

The transform of (10) is

$$\tilde{E}_{\rho(i)}(\zeta, z) = -\frac{1}{j\omega\epsilon_i^*}\frac{\partial\tilde{H}_{\phi(i)}}{\partial z}. \quad (17)$$

The problem reduces to solving (11) in each layer, matching field components at the boundaries of each layer, and then taking the inverse Hankel transform. The boundary conditions yield relations between the coefficients. In Region 2 the transformed solution in (11) is a damped sinusoid,

$$\tilde{H}_{\phi(2)}(\zeta, z) = A\exp(-\gamma_2(z - d)) + B\exp(\gamma_2(z - d)) \quad (18)$$

and in Region 3 the solution is also a superposition of forward and backward traveling waves of the form

$$\tilde{H}_{\phi(3)}(z) = E\exp(-\gamma_3(z-d)) + F\exp(\gamma_3(z-d)). \quad (19)$$

In the case of semi-infinite media, as $L \to \infty$, $F \to 0$ in order to satisfy physical constraints. In the termination material

$$\tilde{H}_{\phi(4)}(z) = H\exp(-\gamma_4(z-d)). \quad (20)$$

B. Fields in Coaxial Line

Since the Laplacian is separable, the solution to the normalized radial electric field in the coaxial line can be written as a linear combination of TEM and TM_{0n} modes:

$$E_{\rho(1)}(\rho,z) = \underbrace{[\exp(-\gamma_1 z) + \Gamma_0\exp(\gamma_1 z)]R_0(\rho)}_{\text{TEM}} + \sum_{n=1}^{\infty}\underbrace{\Gamma_n\exp(\gamma_{n(c)}z)R_n(\rho)}_{\text{TM}_{0n}} \quad (21)$$

for $a \le \rho \le b$ and zero for values of ρ outside this region. In the coaxial line $\gamma_1 = j\omega\sqrt{\epsilon^*_{\text{Rc}}\mu^*_{\text{Rc}}}/c_{\text{vac}}$. The coaxial line TM_{0n} propagation constants are

$$\gamma_{n(c)} = j\sqrt{(\omega/c_{\text{vac}})^2\epsilon^*_{\text{Rc}}\mu^*_{\text{Rc}} - k^2_{n(c)}}. \quad (22)$$

Using appropriate signs for evanescent waves, $\gamma_{0(c)} = \gamma_1$ and, Γ_n is the reflection coefficient of the nth mode. The ground plane that connects to the outer conductor of the coaxial probe is assumed to extend to infinity in the radial direction. At the inner and outer conducting surfaces of the coaxial line, the tangential electric field E_z for the TM_{0n} modes must approach zero. The z-component of the electric field is given by

$$E_z = \frac{1}{j\omega\epsilon^*}\left[\frac{\partial H_\phi(\rho,z)}{\partial\rho} + \frac{1}{\rho}H_\phi(\rho,z)\right] \quad (23)$$

Therefore the radial eigenfunctions in the coaxial line that satisfy the correct boundary conditions on TM_{0n} modes on the inner and outer conductors are

$$R_n(\rho) = \underbrace{C_0/\rho}_{\text{for } n=0 \text{ (TEM mode)}} = \underbrace{C_n[J_1(k_{n(c)}\rho)N_0(k_{n(c)}a) - N_1(k_{n(c)}\rho)J_0(k_{n(c)}a)]}_{n>0(\text{TM}_{0n}\text{ modes})} \quad (24)$$

where N_i are the Bessel functions of the second kind and the constants C_n are obtained by requiring orthogonality [4], [11]:

$$\int_a^b \zeta R_m(b\zeta)R_n(a\zeta)d\zeta = \delta_{\text{mn}},\ m,n = 0,1,2\ldots. \quad (25)$$

Therefore

$$C_0 = \frac{1}{\sqrt{\ln(b/a)}} \quad (26)$$

and

$$C_n = \sqrt{\frac{1}{\int_a^b \rho R_n^2(\rho)d\rho}} = \frac{\pi k_{n(c)}}{\sqrt{2}}\frac{1}{\sqrt{\frac{J_0^2(k_{n(c)}a)}{J_0^2(k_{n(c)}b)} - 1}}. \quad (27)$$

Unless stated otherwise we will assume that the radial eigenfunctions are normalized. The eigenvalues $k_{n(c)}$ are obtained from the condition of vanishing tangential electric field on the conductor walls. The tangential electric field is given by (23). These are the nth solutions of

$$[J_0(k_{n(c)}a)N_0(k_{n(c)}b) - N_0(k_{n(c)}a)J_0(k_{n(c)}b)] = 0. \quad (28)$$

The functions $R_n(r)$ satisfy a Sturm-Liouville problem, which yields Bessel functions. The radial eigenfunctions are orthogonal over $[a, b]$ with respect to the weighting function ρ. The procedure is to perform the Hankel transform on (21) to allow the matching of the transformed fields in the axial coordinate. The transformed radial electric field in the coaxial line is

$$\tilde{E}_{\rho(1)}(\zeta,z) = D_0[\exp(-\gamma_1 z) + \Gamma_0\exp(\gamma_1 z)] + \sum_{n=1}^{\infty}\Gamma_n D_n\exp(\gamma_{n(c)}z). \quad (29)$$

The coefficients $D_n(\zeta) = \int_a^b \rho J_1(\zeta\rho)R_n(\rho)d\rho$ can be found analytically. For $n = 0$

$$D_0(\zeta) = \frac{1}{\sqrt{\ln b/a}}\int_a^b J_1(\zeta\rho)d\rho = \frac{1}{\sqrt{\ln b/a}}\frac{1}{\zeta}[J_0(\zeta a) - J_0(\zeta b)] \quad (30)$$

and otherwise

$$D_n(\zeta) = \int_a^b \rho R_n(\rho)J_1(\zeta\rho)d\rho = \frac{2}{\pi}\frac{C_n}{k_{n(c)}}\frac{1}{J_0(k_{n(c)}b)}\frac{\zeta}{k^2_{n(c)} - \zeta^2} \times [J_0(\zeta b)J_0(k_{n(c)}a) - J_0(\zeta a)J_0(k_{n(c)}b)]. \quad (31)$$

The azimuthal magnetic field in the coaxial line can be found from Maxwell's equations:

$$H_{\phi(1)}(\rho,z) = -\frac{j\omega\epsilon_0\epsilon^*_{\text{Rc}}}{\gamma_1}R_0(\rho) \times [-\exp(-\gamma_1 z) + \Gamma_0\exp(\gamma_1 z)] - j\omega\epsilon_0\epsilon^*_{\text{Rc}}\sum_{n=1}^{\infty}\frac{1}{\gamma_{n(c)}}\Gamma_n\exp(\gamma_{n(c)}z)R_n(\rho). \quad (32)$$

Therefore the transformed magnetic field is

$$\tilde{H}_{\phi(1)}(\zeta,z) = -\frac{D_0 j\omega\epsilon_0\epsilon^*_{\mathrm{Rc}}}{\gamma_1} \times [-\exp(-\gamma_1 z) + \Gamma_0 \exp(\gamma_1 z)] - j\omega\epsilon_0\epsilon^*_{\mathrm{Rc}} \sum_{n=1}^{\infty} \frac{1}{\gamma_{n(c)}} \Gamma_n \exp(\gamma_{n(c)} z) D_n. \tag{33}$$

C. Field Matching at Interfaces

The tangential component of the transformed electric field is continuous across the coaxial line-air gap interface. Therefore from (18) and (29) and the impedance relationship for TM modes,

$$(1+\Gamma_0)D_0 + \sum_{n=1}^{\infty} \Gamma_n D_n = -\frac{\gamma_2}{j\omega\epsilon^*_g}(-A\exp(\gamma_2 d) + B\exp(-\gamma_2 d)). \tag{34}$$

The tangential component of the magnetic field is also continuous across this interface; from (18) and (33),

$$D_0(\zeta)(1-\Gamma_0)\frac{j\omega\epsilon_0\epsilon^*_{Rc}}{\gamma_1} - j\omega\epsilon_0\epsilon^*_{Rc}\sum_{n=1}^{\infty}\frac{1}{\gamma_{n(c)}}\Gamma_n D_n = A\exp(\gamma_2 d) + B\exp(-\gamma_2 d). \tag{35}$$

At the interface between the air gap and the sample we also have continuity of the tangential components; from (18) and (19),

$$A + B = E(1+\Theta) \tag{36}$$

$$\frac{\gamma_2}{\epsilon^*_{\mathrm{Rg}}}(B-A) = \frac{\gamma_3 E}{\epsilon^*_{\mathrm{Rs}}}(\Theta - 1). \tag{37}$$

For a shorted termination at $z = d + L$, $\Theta = \exp(-2\gamma_3 L)$. For a material termination at this position we define $\Theta = \exp(-2\gamma_3 L)(1-\Theta_2)/(1+\Theta_2)$, where $\Theta_2 = (\epsilon^*_{\mathrm{Rs}}\gamma_4)/(\epsilon^*_{Rd}\gamma_2)$. In the limit of semi-infinite material, $L \to \infty$ and since $\epsilon''_{\mathrm{Rs}} > 0$ we obtain $\Theta \to 0$.

We can solve (34), (36), and (37) simultaneously for the unknown coefficients A, B, E, obtaining (38)–(40), shown at the bottom of the page.

An expression for the reflection coefficient Γ_n of the TEM and TM_{0n} modes can be found by taking the inverse transform of (35) in the radial coordinate:

$$R_0(\rho)\frac{j\omega\epsilon_0\epsilon^*_{Rc}}{\gamma_1} - \sum_{n=0}^{\infty}\frac{j\omega\epsilon_0\epsilon^*_{Rc}}{\gamma_{n(c)}}\Gamma_n R_n(\rho) = \int_0^{\infty}\zeta J_1(\zeta\rho)[A\exp(\gamma_2 d) + B\exp(-\gamma_2 d)]d\zeta. \tag{41}$$

In order to obtain Γ_0 we multiply this equation by $\rho R_m(\rho)$ on both sides and integrate this equation over $[a,b]$:

$$\frac{j\omega\epsilon_0\epsilon^*_{\mathrm{Rc}}}{\gamma_m}\Gamma_m = -\int_0^{\infty}\zeta D_m[Ae^{\gamma_2 d} + Be^{-\gamma_2 d}]d\zeta + \frac{j\omega\epsilon_0\epsilon^*_{\mathrm{Rc}}}{\gamma_1}\delta_{m0}. \tag{42}$$

Therefore in matrix form we can write

$$\mathbf{Q}\cdot\vec{\Gamma} = \vec{P}, \tag{43}$$

or

$$\sum_{n=0}^{\infty} Q_{mn}\Gamma_n = P_m \tag{44}$$

where the equations at the bottom of the next page (45)–(46) hold for $m, n = 0, 1, 2, \cdots, N$. The reflection coefficient of the TEM mode is of primary interest since the other modes are evanescent in the coaxial line.

The z-component of the electric field is found from (22). The Bessel function relationship may be used for the derivatives:

$$\frac{dJ_1(\zeta\rho)}{\zeta d\rho} = J_0(\zeta\rho) - \frac{1}{\zeta\rho}J_1(\zeta\rho). \tag{47}$$

In region (2),

$$E_{z(2)}(\rho,z) = \frac{1}{j\omega\epsilon_g}\left[\int_0^{\infty}\zeta^2 J_0(\zeta\rho)[A\exp(-\gamma_2(z-d)) + B\exp(\gamma_2(z-d))]d\zeta\right]. \tag{48}$$

$$A = \frac{j\omega\epsilon_0\epsilon^*_{\mathrm{Rg}}\exp(\gamma_2 d)(\sum_{n=0}^{\infty}\Gamma_n D_n + D_0)((\epsilon^*_{\mathrm{Rs}}\gamma_2 + \epsilon^*_{\mathrm{Rg}}\gamma_3) + \Theta(\epsilon^*_{\mathrm{Rs}}\gamma_2 - \epsilon^*_{\mathrm{Rg}}\gamma_3))}{\gamma_2(\exp(2\gamma_2 d)((\epsilon^*_{\mathrm{Rs}}\gamma_2 + \epsilon^*_{\mathrm{Rg}}\gamma_3) + \Theta(\epsilon^*_{\mathrm{Rs}}\gamma_2 - \epsilon^*_{\mathrm{Rg}}\gamma_3) + (\epsilon^*_{\mathrm{Rg}}\gamma_3 - \epsilon^*_{\mathrm{Rs}}\gamma_2) - \Theta(\epsilon^*_{\mathrm{Rs}}\gamma_2 + \epsilon^*_{\mathrm{Rg}}\gamma_3)))} \tag{38}$$

$$B = \frac{j\omega\epsilon_0\epsilon^*_{\mathrm{Rg}}\exp(\gamma_2 d)(\sum_{n=0}^{\infty}\Gamma_n D_n + D_0)((\epsilon^*_{\mathrm{Rs}}\gamma_2 - \epsilon^*_{\mathrm{Rg}}\gamma_3) + \Theta(\epsilon^*_{\mathrm{Rs}}\gamma_2 + \epsilon^*_{\mathrm{Rg}}\gamma_3))}{\gamma_2((\exp(2\gamma_2 d)(\epsilon^*_{\mathrm{Rs}}\gamma_2 + \epsilon^*_{\mathrm{Rg}}\gamma_3) + \Theta(\epsilon^*_{\mathrm{Rs}}\gamma_2 - \epsilon^*_{\mathrm{Rg}}\gamma_3) + (\epsilon^*_{\mathrm{Rg}}\gamma_3 - \epsilon^*_{\mathrm{Rs}}\gamma_2) - \Theta(\epsilon^*_{\mathrm{Rs}}\gamma_2 + \epsilon^*_{\mathrm{Rg}}\gamma_3)))} \tag{39}$$

$$E = \frac{2j\omega\epsilon_0\epsilon^*_{\mathrm{Rs}}\epsilon^*_{\mathrm{Rg}}\exp(\gamma_2 d)(\sum_{n=0}^{\infty}\Gamma_n D_n + D_0)}{\exp(2\gamma_2 d)((\epsilon^*_{\mathrm{Rs}}\gamma_2 + \epsilon^*_{\mathrm{Rg}}\gamma_3) + \Theta(\epsilon^*_{\mathrm{Rs}}\gamma_2 - \epsilon^*_{\mathrm{Rg}}\gamma_3) + (\epsilon^*_{\mathrm{Rg}}\gamma_3 - \epsilon^*_{\mathrm{Rs}}\gamma_2) - \Theta(\epsilon^*_{\mathrm{Rs}}\gamma_2 + \epsilon^*_{\mathrm{Rg}}\gamma_3)))} \tag{40}$$

The radial electric field is

$$E_{\rho(2)}(\rho,z) = -\frac{1}{j\omega\epsilon_g}\int_0^\infty \zeta\gamma_2 J_1(\zeta\rho)[-A\exp(-\gamma_2(z-d)) + B\exp(\gamma_2(z-d))]d\zeta. \quad (49)$$

Similar equations exist for the region 3.

III. Uncertainty Analysis

Uncertainties in open-ended coaxial measurements include calibration and measurement errors. Here we consider the uncertainty in a measurement due to phase, magnitude and lift-off. We consider that calculated permittivity is a function of the following independent variables: $\epsilon^*_{\mathrm{Rs}}(|\Gamma_i|,\theta_i,d)$, where i denotes measurement standards and coaxial line. The estimated magnitude and phase uncertainties introduced by the measurement standards are combined with the network analyzer uncertainties. A worst-case differential uncertainty analysis assuming no cross-correlations requires that

$$\Delta\epsilon'_{\mathrm{Rs}} = \sqrt{\sum_i\left[\left(\frac{\partial\epsilon'_{\mathrm{Rs}}}{\partial|\Gamma_i|}\Delta|\Gamma_i|\right)^2+\left(\frac{\partial\epsilon'_{\mathrm{Rs}}}{\partial\theta_i}\Delta\theta_i\right)^2\right]+\left(\frac{\partial\epsilon'_{\mathrm{Rs}}}{\partial d}\Delta d\right)^2}. \quad (50)$$

A similar equation exists for ϵ''_{Rs}. Implicit differentiation can be used to find the necessary derivatives:

$$\frac{\partial\epsilon^*_{\mathrm{Rs}}}{\partial|\Gamma_i|} = \frac{\exp(j\theta_i)}{\frac{\partial\Gamma_i}{\partial\epsilon^*_{\mathrm{Rs}}}} \quad (51)$$

$$\frac{\partial\epsilon^*_{\mathrm{Rs}}}{\partial\theta_i} = j|\Gamma_i|\frac{\exp(j\theta_i)}{\frac{\partial\Gamma_i}{\partial\epsilon^*_{\mathrm{Rs}}}} \quad (52)$$

$$\frac{\partial\epsilon^*_{\mathrm{Rs}}}{\partial d} = -\sum_i \frac{\frac{\partial\Gamma_i}{\partial d}}{\frac{\partial\Gamma_i}{\partial\epsilon^*_{\mathrm{Rs}}}}. \quad (53)$$

A two-dimensional uncertainty plot is shown in Fig. 2. We see generally an increase in uncertainty as lift-off increases and frequency decreases, however not always.

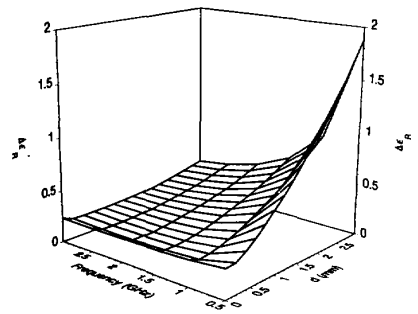

Fig. 2. Two-dimensional plot of the combined uncertainty in ϵ'_{Rs}. The parameters used were $\epsilon^*_{\mathrm{Rs}} = (10,-.01)$, six TM_{0n} modes, $\Delta d = 0.000254$ m, $\Delta\theta = 0.5°$, $\Delta|\Gamma_0| = 0.002$.

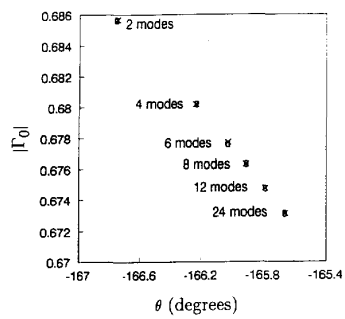

Fig. 3. The magnitude of the reflection coefficient for $d = 0$ versus phase at 1 GHz for $a = 2.333$ mm and $b = 7.549$ mm, $\epsilon^*_{\mathrm{Rc}} = 2.15$, with $\epsilon^*_{\mathrm{Rs}} = (100,-100)$ where x denotes current paper results and 0 denotes Hodgetts' results.

IV. Numerical Results

In order to check the analytical model a number of numerical solutions were generated. In Fig. 3 we compare our solution for the special case of no lift-off to the results of Hodgetts [13], [14]. In this limit, the agreement is excellent.

Knowledge of the variation of the reflection coefficient as a function of lift-off is very important for many applications. In Figs. 4 and 5 we plot the variation of the magnitude and phase of the reflection coefficient as a function of lift-off over a lossy

$$Q_{mn} = \int_0^\infty \zeta D_m \frac{\epsilon^*_{\mathrm{Rg}} D_n(e^{2\gamma_2 d}((1+\frac{\epsilon^*_{\mathrm{Rg}}\gamma_3}{\epsilon^*_{\mathrm{Rs}}\gamma_2})+\Theta(1-\frac{\epsilon^*_{\mathrm{Rg}}\gamma_3}{\epsilon^*_{\mathrm{Rs}}\gamma_2}))+((1-\frac{\epsilon^*_{\mathrm{Rg}}\gamma_3}{\epsilon^*_{\mathrm{Rs}}\gamma_2})+\Theta(1+\frac{\epsilon^*_{\mathrm{Rg}}\gamma_3}{\epsilon^*_{\mathrm{Rs}}\gamma_2})))}{\epsilon^*_{\mathrm{Rc}}\gamma_2(e^{2\gamma_2 d}((1+\frac{\epsilon^*_{\mathrm{Rg}}\gamma_3}{\epsilon^*_{\mathrm{Rs}}\gamma_2})+\Theta(1-\frac{\epsilon^*_{\mathrm{Rg}}\gamma_3}{\epsilon^*_{\mathrm{Rs}}\gamma_2}))+((\frac{\epsilon^*_{\mathrm{Rg}}\gamma_3}{\epsilon^*_{\mathrm{Rs}}\gamma_2}-1)-\Theta(1+\frac{\epsilon^*_{\mathrm{Rg}}\gamma_3}{\epsilon^*_{\mathrm{Rs}}\gamma_2})))} d\zeta + \frac{1}{\gamma_{n(c)}}\delta_{mn} \quad (45)$$

$$P_m = -\int_0^\infty \zeta D_m \frac{\epsilon^*_{\mathrm{Rg}} D_0(e^{2\gamma_2 d}((1+\frac{\epsilon^*_{\mathrm{Rg}}\gamma_3}{\epsilon^*_{\mathrm{Rs}}\gamma_2})+\Theta(1-\frac{\epsilon^*_{\mathrm{Rg}}\gamma_3}{\epsilon^*_{\mathrm{Rs}}\gamma_2}))+((1-\frac{\epsilon^*_{\mathrm{Rg}}\gamma_3}{\epsilon^*_{\mathrm{Rs}}\gamma_2})+\Theta(1+\frac{\epsilon^*_{\mathrm{Rg}}\gamma_3}{\epsilon^*_{\mathrm{Rs}}\gamma_2})))}{\epsilon^*_{\mathrm{Rc}}\gamma_2(e^{2\gamma_2 d}((1+\frac{\epsilon^*_{\mathrm{Rg}}\gamma_3}{\epsilon^*_{\mathrm{Rs}}\gamma_2})+\Theta(1-\frac{\epsilon^*_{\mathrm{Rg}}\gamma_3}{\epsilon^*_{\mathrm{Rs}}\gamma_2}))+((\frac{\epsilon^*_{\mathrm{Rg}}\gamma_3}{\epsilon^*_{\mathrm{Rs}}\gamma_2}-1)-\Theta(1+\frac{\epsilon^*_{\mathrm{Rg}}\gamma_3}{\epsilon^*_{\mathrm{Rs}}\gamma_2})))} d\zeta + \frac{1}{\gamma_1}\delta_{m0} \quad (46)$$

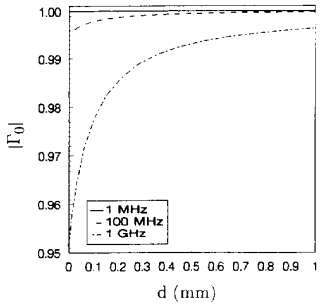

Fig. 4. The magnitude of the reflection coefficient as a function of lift-off for various frequencies of a slab occupying the lower half space. The probe is assumed to have $b = 14$ mm and $a = 6.08$ mm with $\epsilon^*_{\mathrm{R}c} = 2.54$, $\epsilon^*_{\mathrm{R}s} = (10, -1)$, and six TM_{0n} modes were used.

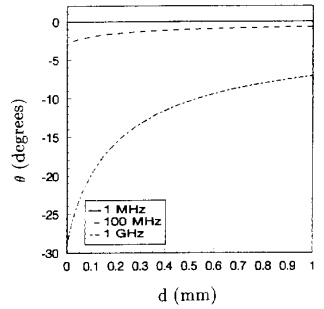

Fig. 5. The phase of the reflection coefficient in degrees as a function of lift-off for various frequencies of a slab occupying the lower half space. The simulation uses $b = 14$ mm and $a = 6.08$ mm with $\epsilon^*_{\mathrm{R}c} = 2.54$, $\epsilon^*_{\mathrm{R}s} = (10, -1)$, and six TM_{0n} modes were used.

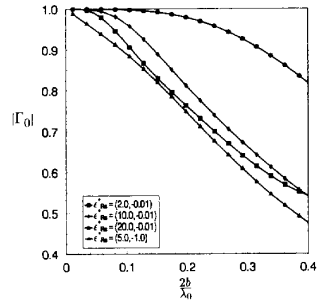

Fig. 6. The magnitude of the reflection coefficient as a function of coaxial line outer conductor radius, normalized to wavelength in air, of a slab of varying dielectric parameters occupying the lower half space. The computation uses $b = 14$ mm and $a = 6.08$ mm with $\epsilon^*_{\mathrm{R}c} = 2.54$, $\epsilon^*_{\mathrm{R}s} = (10, -1)$, zero lift-off, and six TM_{0n} modes were used.

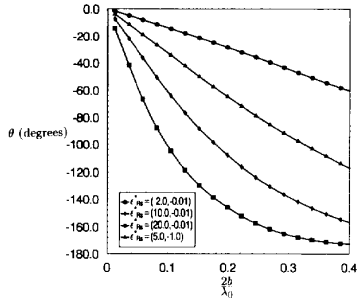

Fig. 7. The phase in degrees as a function of coaxial line outer conductor radius, normalized to wavelength in air, of a slab of varying dielectric parameters occupying the lower half space. The computation uses $b = 35$ mm and $b/a = 2.3$, zero lift-off, and six TM_{0n} modes were used.

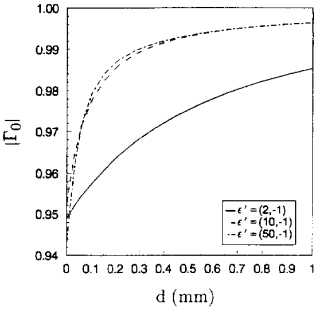

Fig. 8. Magnitude of the reflection coefficient as a function of lift-off for various permittivities of a slab occupying the lower half space. Frequency is 1 GHz, $b = 35$ mm, $b/a = 2.3$, and six TM_{0n} modes were used.

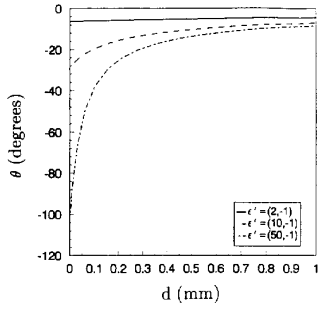

Fig. 9. Phase of the reflection coefficient in degrees as a function of lift-off for various permittivities of a slab occupying the lower half space. Frequency is 1 GHz, $b = 14$ mm, $a = 6.08$ mm, $\epsilon^*_{\mathrm{R}c} = 2.54$, and six TM_{0n} modes were used.

dielectric. The reflection coefficient approaches 1 as lift-off increases. The approach to 1 is slower for higher frequencies. In Fig. 5, we see that the phase of the reflection coefficient approaches 0 as lift-off increases for the lower frequency measurements. At 1 GHz the phase does not attain 0. In Figs. 6 and 7 we plot the variation of the magnitude and phase of the reflection coefficient as a function of coaxial line size. We see from Figs. 8 and 9 that even small air gaps can influence the solution greatly for high dielectric constant materials. Surface wave phenomena are also possible. The electrical size of the coaxial line determines the field penetration from the end of the probe. For $\lambda \gg b - a$ the extrusion of the fields is minimal. In order for open-ended coaxial probes to operate effectively with lift-off, either larger probes or higher frequencies should be used. Waveguide modes can be excited.

Figs. 10 and 11 show a measurement of reflection coefficient as a function of frequency. The results are compared to the theory. We see good overall agreement. Higher lift-off measurements agree better with theoretical predictions than lower lift-off measurements.

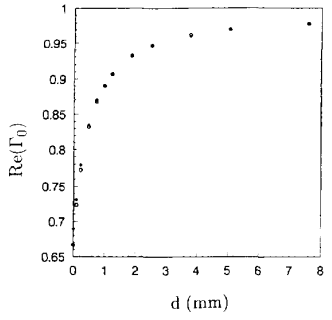

Fig. 10. The real part of the reflection coefficient as a function of lift-off compared with theory, $\epsilon^*_{\mathrm{R}_c} = 2.54$, $\epsilon^*_{\mathrm{R}_s} = (6.15, -.029)$, and six TM_{0n} modes were used. The o denotes experimental values. The combined standard uncertainty at zero lift-off due to the uncertainty in lift-off is $u_c = 0.045$.

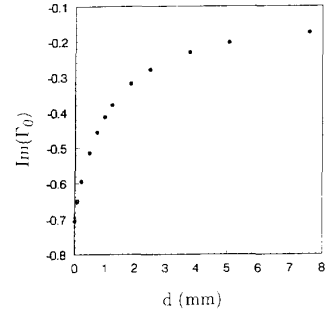

Fig. 11. The imaginary part of the reflection coefficient as a function of lift-off compared with theory, $\epsilon^*_{\mathrm{R}_c} = 2.54$, $\epsilon^*_{\mathrm{R}_s} = (6.15, -.029)$, and six$\mathrm{TM}_{0n}$ modes were used. The o denote experimental values. The combined standard uncertainty at zero lift-off due to the uncertainty in lift-off is $u_c = 0.045$.

In order to obtain simultaneous measurements of permittivity and permeability two independent measurements must be made. This is accomplished for thin materials by measuring the material with and without a short-circuit backing. The short-circuit termination induces a stronger magnetic field than when an open circuit is used. Another approach is to measure the material with two different lift-off positions. The two measured scattering parameters are then used to form two equations in two unknowns. As a typical magnetic measurement, the measured permeability of a ferrite using the probe at zero lift-off was $\mu^*_R = (.011, -4.7)$.

V. Conclusion

In this paper we have developed a model for the electromagnetic response of a coaxial probe with lift-off. The model incorporates a finite gap and finite sample thickness into the coaxial probe theory. The model is useful only to the extent that the experiments adhere to the underlying assumptions. For example, the probe used in the experiments has only a finite ground plane; also, the sample is considered to be infinitely long in the radial direction. Good agreement was obtained between measurements and theoretical predictions for the case of a semi-infinite sample with lift-off. The model was also shown to compare very well with published results at zero lift-off. In order to increase interaction of the fields with the material under test either large diameter probes or higher frequencies need to be used.

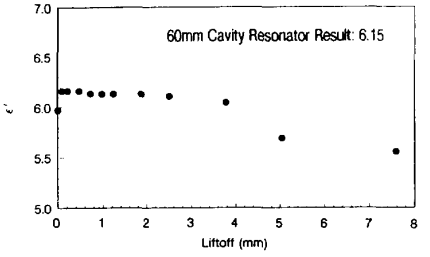

Fig. 12. The real part of the permittivity for a glass sample as obtained from the inverse problem using measured reflection coefficient.

The analysis can be used to optimize probe size for a particular nondestructive application. Probes with lift-off should be useful for nondestructive material property testing and material thickness testing. These types of probes could be particularly useful for nondestructive testing of substrates.

Acknowledgment

The authors would like to thank Dr. George Birnbaum, Dr. Thomas Yolken, and Dr. Alfred Van Clark for support.

References

[1] N. Marcuvitz, *Waveguide Handbook*. New York: Dover Publications, 1951.
[2] J. Galejs, *Antennas in Homogeneous Media*. Oxford, U.K.: Pergamon, 1969.
[3] L. Lewin, *Advanced Theory of Waveguides*. London, U.K.: Iliffe, 1951.
[4] J. R. Mosig, J. E. Besson, M. G. Fabry, and F. E. Gardiol, "Reflection of an open-ended coaxial line and application to non-destructive measurement of materials," *IEEE Trans. Instrum. Meas.*, v ol. IM-30, pp. 46–51, 1981.
[5] M. A. Stuchly and S. S. Stuchly, "Coaxial line reflection methods for measuring dielectric properties of biological substances at radio and microwave frequencies—A review," *IEEE Trans. Instrum. Meas.*, vol. IM-29, pp. 176–183, 1980.
[6] D. Blackham, "Use of open-ended coaxial probe to determine permittivity," in *Microwave Power Symp.*, International Microwave Power Institute, Aug. 1990, pp. 44–45.
[7] L. L. Li, N. H. Ismail, L. S. Taylor, and C. C. Davis, "Flanged coaxial microwave probes for measuring thin moisture layers," *IEEE Trans. Biomedical Eng.*, vol. 39, pp. 49–57, Jan. 1992.
[8] S. Fan, K. Staebell, and D. Misra, "Static analysis of an open-ended coaxial line terminated by layered dielectric," *IEEE Trans. Instrum. Meas.*, vol. 39, pp. 435–437, Apr. 1990.
[9] P. D. Langhe, K. Blomme, L. Martens, and D. D. Zutter, "Measurement of low-permittivity materials based on a spectral domain analysis for the open-ended coaxial probe," *IEEE Trans. Instrum. Meas.*, vol. 42, pp. 879–886, Oct. 1993.
[10] L. S. Anderson, G. B. Gajda, and S. S. Stuchly, "Analysis of open-ended coaxial line sensor in layered dielectric," *IEEE Trans. Instrum. Meas.*, vol. 35, pp. 13–18, Mar. 1986.
[11] H. Levine and C. H. Papas, "Theory of the circular diffraction antenna," *J. Appl. Phys.*, vol. 22, pp. 29–43, Jan. 1951.
[12] J. Baker-Jarvis and R. G. Geyer, "Nondestructive testing with a coaxial probe," in *URSI Dig.*, URSI, Boulder, CO, Jan. 1992.
[13] T. E. Hodgetts, "The open-ended coaxial line: A rigorous variational treatment," Royal Signals and Radar Establishment Memo. 4331, Royal Signals and Radar Establishment, 1989.
[14] S. Jenkins, T. E. Hodgetts, G. T. Symm, A. G. P. Warhamm, and R. N. Clarke, "Comparison of three numerical treatments for the open-ended coaxial line sensor," *Elect. Lett.*, vol. 24, pp. 234&nd ash;235, 1992.
[15] A. P. Gregory, R. N. Clarke, T. E. Hodgetts, and G. T. Symm, "Rf and microwave dielelctric measurements upon layered materials using a reflectometric coaxial sensor," Tech. Rep. NPL Rep. DES 125, National Physical Laboratory, Mar. 1993.

James Baker-Jarvis (M'89–SM'90) received the B.S. degree in mathematics in 1975. His received the Masters degree in physics in 1980 from the University of Minnesota, and the Ph.D. degree in theoretical physics in 1984 from the University of Wyoming.

He worked as an AWU postdoctoral fellow after graduation for one year on theoretical and experimental aspects of intense electromagnetic fields in lossy materials and dielectric measurements. He then spent two years as a temporary Assistant Professor in the Physics Department at the University of Wyoming, where he was leader of a group on electromagnetic heating processes, taught classes, and performed research on electromagnetic propagation in lossy materials. Then through 1988 he was Assistant Professor of Physics at North Dakota State University. He joined the National Institute of Standards and Technology, Boulder, CO, in January 1989, where his interests are in the areas of materials, dielectric and magnetic spectroscopy, and nondestructive evaluation. He is the author of numerous publications in such diverse areas of dielectric and magnetic measurements, electromagnetics, kinetic theory of fracture, hydrodynamics, heat transfer, maximum-entropy methods, and numerical modeling.

Dr. Baker-Jarvis is a NIST Bronze Medal recipient, a member of the American Physical Society, and the American Association of Physics Teachers.

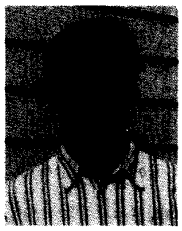

Michael D. Janezic (M'91) received the B.S. degree in electrical engineering from the University of Colorado in 1991. He is currently working on the M.S. degree, specializing in electromagnetic theory, maximum-entropy methods, and solid-state physics.

Since 1988 he has worked in the Electromagnetic Fields Division at the National Institute of Standards and Technology, Boulder, CO. His research interests include complex permittivity and permeability measurements of solid and liquid materials using cavity resonator and transmission line techniques.

Mr. Janezic is a member of Tau Beta Pi and Eta Kappa Nu.

Paul D. Domich received the B.S. degree in mathematics from the University of Colorado in 1979, the M. S. degree in 1983, and the Ph.D. degree in 1985 from Cornell University in operations research. He was a postdoctoral fellow at the Université de Louvain, Louvain-la-Neuve, Belgium, in 1986. He has been a mathematician at National Institute of Standards and Technology, Boulder, CO since 1977 and is currently a senior mathematician of the Applied and Computational Mathematics Division in the Computing and Applied Mathematics Laboratory of NIST.

Dr. Domich is a member of the Operations Research Society of America.

Richard G. Geyer (M'87–SM'87) received the B. Sc. (honors) and Ph. D. degrees in 1966 and 1970 from Michigan State University and Colorado School of Mines, respectively.

Since 1970 he has been involved with electronic properties of material measurements and with numerical methods of electromagnetic and acoustic field theory. Since 1986, he has been at the National Institute of Standards and Technology, Boulder, CO, within the Antenna and Electromagnetic Properties of Materials Metrology group, where his research deals mainly with theory and applications of dielectric waveguides, dielectric resonators, microwave ferrites, and measurements of the dielectric and magnetic properties of materials at microwave frequencies.

In 1972, Dr. Geyer was given a best paper award for transient electromagnetic scattering in an inhomogeneous penetrable half space.